ARCHIVES OF ELECTRICAL ENGINEERING VOL. 70(1), pp. 233–244 (2021)

DOI 10.24425/aee.2021.136064

Influence of thermal-mechanical stress on the insulation system of a low voltage electrical machine

LIGUO YANG, FLORIAN PAULI, KAY HAMEYER

Institute of Electrical Machines (IEM), RWTH Aachen University
Schinkelstraße 4, 52062 Aachen, Germany
e-mail: liguo.yang@iem.rwth-aachen.de

(Received: 18.11.2020, revised: 23.12.2020)

Abstract: Varying ohmic loss in the winding of electrical machines, which are operated at various operating points, results in temperature changes during operation. Particularly, when the temperature is varying dynamically, the insulation system suffers from repeated thermal-mechanical stress, since the thermal expansion coefficients of the insulating materials and copper conductors are different. For the appropriate design of an insulation system, the effect of thermal-mechanical stress must be known. In the present work, motorettes are subjected to repeated thermal cycles. The expected lifetime is estimated and compared to the lifetime which is achieved by applying a lifetime-model which only considers thermal aging while ignoring thermal-mechanical stress effects. In addition, the hotspot temperature is simulated, the lifetime at the hotspot is estimated as the worst case. As expected, the results indicate that the thermal-mechanical stress plays a significant role during dynamic thermal aging of the winding insulation system. To better understand the thermal-mechanical stress effect, the resulting thermal-mechanical stress in a single wire is analyzed by the finite element method. A preliminary analysis of the aging mechanism of materials due to cyclic thermal-mechanical stress is performed with the theory of material fatigue.

Key words: hotspot, insulation system, material fatigue, thermal-mechanical stress

1. Introduction

For the design of electrical machines, the quality and behavior of the electrical insulation system are becoming an increasing concern. Fig. 1 [1] shows the setup of the electrical insulation system in a low voltage electrical machine. Since energy loss is inevitable during the operation of the electrical machine, the temperature of the winding rises when the load is increased [2]. When the temperature is varying, the electrical insulation is subjected not only to thermal stress but also

thermal-mechanical stress, which is caused by different coefficients of thermal expansion (CTE) of copper and insulating material. Mechanical stress, especially shear stress, is generated at the interfaces between wire coating and copper as well as between wire coating and impregnation [3, 4].

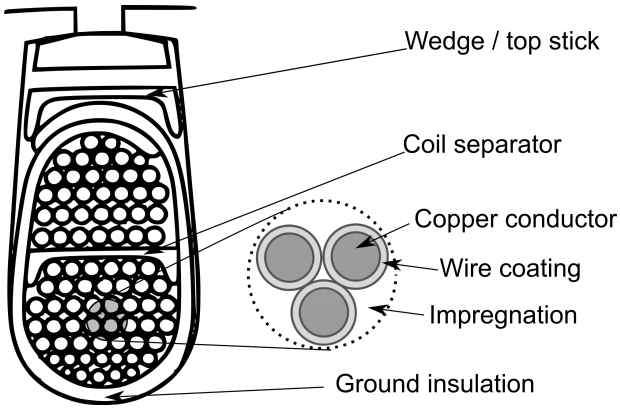

Fig. 1. Setup of the insulation system of a low voltage electrical machine [1]

Failure of the insulation system is usually caused by material degradation with the time of operation. Subsequently, when the material cannot withstand a certain stress level, the whole insulation system fails. In the late 19th century Arrhenius [5] expounded the relation between temperature and the rate of reaction for a single chemical process. Based on this theory, Dakin [6] developed a lifetime model of the insulation system. With the knowledge of the Dakin model, thermal aging of the insulation system at a constant temperature has recently been further studied with consideration of environmental influence [7, 8]. In comparison, less attention has been drawn to the temperature variation. Madonna [9] divided dynamic thermal cycles into finite sections, and a loss fraction of the insulation system at each temperature section is calculated based on the thermal model, thus the entire lifetime is a weight function of temperature. However, the thermal-mechanical stress is still not considered. Sciascera [10] takes the thermal-mechanical stress into consideration, thus, the lifetime is a function of temperature and in particular the temperature variation, while the relation between temperature variation and thermal-mechanical stress is not further analyzed. Huang [3] simulated the thermal mechanical aging process with a finite element model of a single wire, and the lifetime model was correlated with material fatigue. The aforementioned works provides a general view that thermal-mechanical aging plays an important role during the dynamic thermal loading process. It is well known that hotspots develop inside the winding during operation. In the aforementioned works, however, an increased temperature at the hotspot is rarely considered.

The goal of the present work is to study the effect and significance of the thermal-mechanical stress during dynamic thermal loading process. To achieve this goal, the associated thermal aging and thermal-mechanical aging are analyzed separately and compared with the experimental result. Specifically, experiments are conducted to simulate a dynamic thermal aging process and the lifetime of the applied insulation system is estimated. In terms of thermal aging, since high temperature accelerates the aging process significantly, an analysis of temperature distribution, more specifically, the temperature profile in the hotspot is necessary for a precise estimation

of lifetime. Therefore, the temperature profile at hotspots is simulated by means of thermal modeling, the related lifetime is calculated with a lifetime model for the worst case. Subsequently, the significance of the thermal-mechanical stress effect is verified by comparison of experimental and calculated results, while as aforementioned, the simulation only considers thermal aging. To estimate the scale of the thermally induced mechanical stress in the winding, a finite element model of a single wire is setup, and the stress effect is related to the analysis of material fatigue.

2. Experiment and methodology

2.1. Experimental setup

The basic setup of a single motorette is shown in Fig. 2, the material configuration of the insulation system of the motorette is listed in Table 1. To simulate the dynamic thermal load, the average temperature of samples is measured by means of resistance measurement. As indicated in (1), the resistance is dependent on the temperature, where R_0 denotes the resistance at the reference temperature T_0, α stands for the temperature coefficient of resistance and $R(T)$ for the electrical resistance at the temperature T.

$$R(T) = R_0 \cdot [1 + \alpha \cdot (T - T_0)]\,. \tag{1}$$

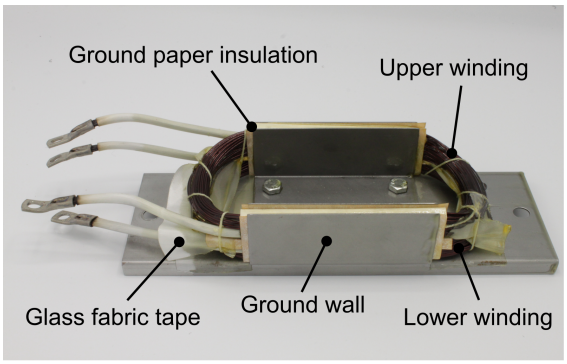

Fig. 2. Motorette of a double-layer winding configuration

Table 1. Material configuration of the insulation system of the motorette

Component	Material
Winding	Damid 200 GR2
Ground paper insulation	Trivoltherm NKN 25 20
Glass fabric tape	Syntape H618/GL.96
Impregnation	Axalta Voltatex 4250

In this study, 7 motorettes ($M_i, i \in \{1, 2 \ldots 7\}$) are connected in series and placed in a climate chamber, a recording system (RS) is connected to a computer (PC) which is equipped with control software, as shown in Fig. 3. The motorettes are heated up with a constant DC current of 200 A and cooled at an ambient temperature of 0°C. The average temperature of 7 motorettes ranges from 90°C to 235°C. The obtained temperature profile via resistance measurement for one thermal cycle is displayed in Fig. 4. It should be noted that the thermal aging process is usually accelerated by means of increasing the aging temperature in the laboratory work. Considering a thermal class of 180°C of these motorettes, a thermal aging temperature of 235°C is acceptable according to the standard IEC 60505 [11].

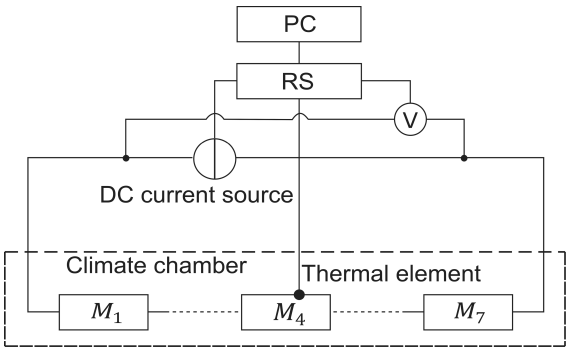

Fig. 3. Schematic of the test bench

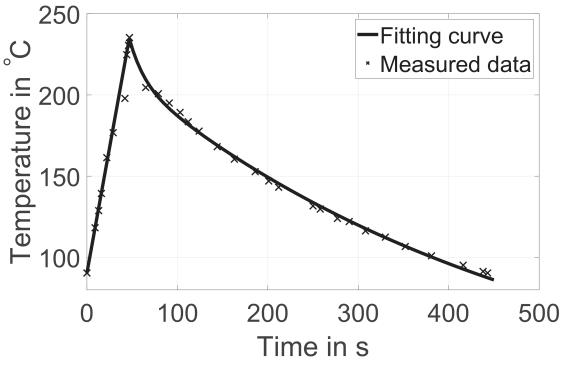

Fig. 4. Measured average temperature profile during one thermal cycle

The resistances of 7 motorettes are measured to be (36.08 ± 1.44) mΩ before the test at room temperature, which indicates that the initial resistances of 7 motorettes are almost the same. Subsequently, the influence of resistance variation on the temperature distribution between 7 motorettes can be neglected. Considering the worst heat dissipation in the middle of the series connected motorettes, additional thermoelements are attached on the endwinding of motorette M_4 for extra temperature monitoring, which however, is proved not to be as reliable as the resistance measurement, since the measured surface temperature is greatly influenced by the environmental condition. Therefore, the measured resistances are used for the temperature analysis in the following work.

2.2. End-of-life (EOL) criterion

The winding insulation system of low voltage electrical machines should be designed to be free of partial discharge (PD) at all operating points, since PD will cause failure within a relatively short time [12, 13]. Therefore, a minimum value for the partial discharge inception voltage (PDIV) is defined as the end-of-life (EOL) criterion for the diagnose of the insulation system. The insulation system, which is analyzed in the present work, is designed to operate in a drive train with a DC-link voltage of 385 V. Applying an overshoot-factor of 1.5 and safety factors according to the standard IEC 60034-18-41 [14], the minimum PDIVs are:

– 1883 V for the phase to phase voltage and
– 1116 V for the phase to ground voltage.

2.3. Thermal aging

According to the Dakin model [6], the lifetime L is a function of the temperature T, as described in (2):

$$L = A \cdot \exp\left(\frac{B}{T}\right), \tag{2}$$

where A and B are constants which can be estimated by accelerated thermal aging.

The Dakin model is suitable for thermal aging at a constant temperature, while for a dynamic thermal load such as in traction motors, the classic Dakin model needs to be modified, since the temperature is varying with time. Assuming that the aging rate is reciprocal to the lifetime, and the loss fraction (LF) of the lifetime can be expressed as a function of temperature. Thus, when the temperature is time-dependent, the LF for one thermal cycle LF_{cycle} can be deduced with (3):

$$LF_{\text{cycle}} = \int_0^{\Delta t_{\text{cycle}}} \mathrm{d}LF = \int_0^{\Delta t_{\text{cycle}}} \frac{1}{L_0} \exp\left[-B\left(\frac{1}{T_0} - \frac{1}{T(t)}\right)\right] \mathrm{d}t, \tag{3}$$

where: L_0 denotes the lifetime by the reference temperature T_0, B the Dakin constant, Δt_{cycle} the time period of one thermal cycle and $T(t)$ the time-dependent temperature.

2.4. Thermal-mechanical stress between bonded layers and material fatigue

As mentioned above, the thermal-mechanical stress is caused by a different coefficient of thermal expansion (CTE) of bonded layers. As shown in Fig. 5 [4], the induced shear stress at the symmetric plane (dash line) is zero. The stress rises gradually along the wire length and reaches its maximum at the free end. The resulting shear stress τ in the joint layer due to a temperature change of ΔT can be expressed as [4]:

$$\tau = \frac{(\alpha_1 - \alpha_2)\, G \Delta T \sinh(\beta x)}{\beta \eta \cosh(\beta l)}, \tag{4}$$

with

$$\beta^2 = \frac{G}{\eta}\left(\frac{1}{E_1 t_1} + \frac{1}{E_2 t_2}\right), \tag{5}$$

where: E_1 and E_2 are the elastic moduli of layer 1 and 2, G is the shear modulus of the joint layer, α_1 and α_2 represent the CTE of layer 1 and 2, l is the length in the x direction, t_1, η and t_2 represent the thicknesses of corresponding layers, respectively. According to [4], τ reaches its maximum at the end of the length l, which is expressed as following:

$$\tau_{\max} = \frac{(\alpha_1 - \alpha_2)\, G\Delta T \tanh(\beta l)}{\beta \eta}. \tag{6}$$

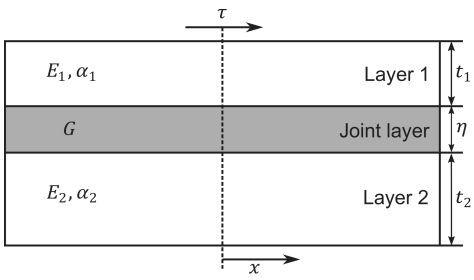

Fig. 5. Demonstration of thermally induced shear stress between bonded layers [4]

Usually it is sufficient to assume that $\tanh(\beta l) \approx 1$, thus, the maximum shear stress $\tau_{\max}$ occurs at the end of the bonded layers while is independent of the total length l, as expressed in (7):

$$\tau_{\max} = \frac{(\alpha_1 - \alpha_2)\, G\Delta T}{\beta \eta}. \tag{7}$$

The analysis above provides an example of the associated mechanical stress in the x direction. Besides, [15] provides a numerical analysis about the associated normal stress between bonded layers. This theory can be linked to the coating wires of the insulation systems. Accordingly, thermal-mechanical stress occurs in the wire coating due to adjacent layers of copper and impregnation. A preliminary analysis of the thermally induced mechanical stress is conducted with the finite element analysis (FEA) method.

Cyclic thermal-mechanical stress causes material fatigue. Even within the elastic deformation region, local deformation accumulates and finally causes failure after a sufficient number of cycles. The stress-life (S-N) model describes the relation between the maximum stress of the cyclic elastic deformation $S_{\max}$ and the required cycles to the failure N, assuming that the cyclic mechanical stress is sinusoidal. Fig. 6 demonstrates a typical tension fatigue curve for a material of PAI 7130 [3]. It should be noted that the values obtained in fatigue testing are influenced by the specimen and testing method. Therefore, the values should serve as guidelines, rather than absolute values.

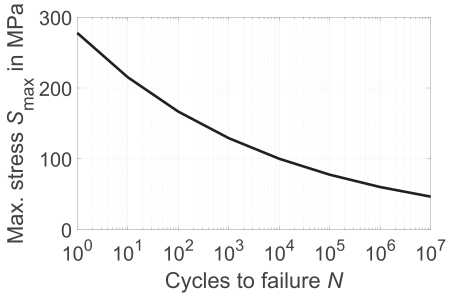

Fig. 6. Tension-fatigue curve of PAI 7130 [3]

3. Results

3.1. Results of measurement

As mentioned in the last section, 7 motorettes are numbered and periodically tested with a *SCHLEICH MTC3* measuring device during this experiment, applying a sinusoidal voltage either between two phases or between phase and ground. The choice and application of a sinusoidal voltage for this experiment is valid according to IEC 60034-18-41 [14]. The voltage (amplitude) starts from 400 V and increases gradually up to 2000 V in steps of 50 V. The samples are tested after each 100 cycles, and after 1900 cycles there is still no failure occurring between phase and ground. Instead, PD is prone to occur initially between windings, the related first failure occurs after 400 cycles. Therefore, the aforementioned phase-to-phase criterion counts for lifetime estimation in the present work. During the tests, phenomena are noticed that some motorettes identified as defective in the last round of testing are again tested to be free of PD within the voltage limit. This may be due to the fact that two defective conductors have direct contact with each other during the first measurement while they are not in direct contact anymore during the second measurement due to mechanical vibration of individual conductors. Nevertheless, the samples are regarded to be defective in this case.

After 1000 cycles, 5 of the 7 tested motorettes fail. In the range of 1000 and 1900 cycles the number of failures stays constant while the remaining 2 motorettes still show no sign of PD within the voltage limit. Considering that it could take a long time for the remaining 2 motorettes to finally fail, which, however, greatly deviates from the others, the measurement stopped after 1900 cycles, and the 5 failed motorettes are used as the size of sampling units for a statistical estimate of their lifetime. It can be understood that the motorettes applied in the present work are wound and impregnated by hand, which can result in significant quality differences. As a consequence, some individual motorettes may run significantly longer than the others. Based on this assumption the loss fraction of their lifetime with respect to thermal cycles are plotted in Fig. 7(b). Here it is necessary to note that even if a total number of 5 samples are applied, the result still meets the minimum requirement of 5 samples according to IEC 60505 [11].

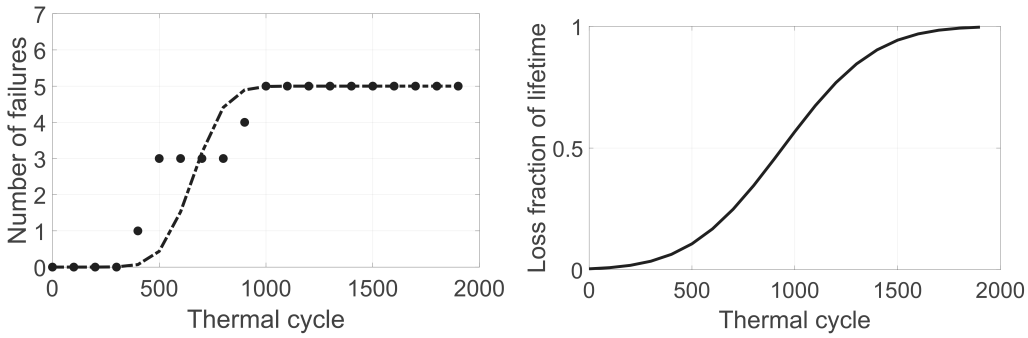

(a) (b)

Fig. 7. Experimental result of (a) number of failures and (b) loss fraction of lifetime with respect to thermal cycles

Material degradation obeys generally normal distribution, and based on that the average lifetime $\overline{L}$ as well as lifetime with 95% confidence L_{95} are estimated and summarized in Table 2. The experimental results will be compared with results of the numerical analysis in the following subsection.

3.2. Thermal modeling of hotspot behavior and lifetime estimation

The temperature distribution inside the windings is greatly dependent on the frequency and the heating rate of thermal cycles. For a low frequency thermal cycle with a low heating rate, the temperature distribution is usually regarded as homogeneous. For example, [7,8] conduct thermal aging under constant temperature. During the process, motorettes are placed in drying kilns and maintained at constant temperatures. Besides, the heating and cooling rate are also relatively low, therefore, the temperatures across the windings are almost the same. In this case, there is no need to consider the issue of hotspots. However, when motorettes are heated and cooled in a short time period, a temperature gradient is inevitable and hotspots must be considered for the worst case, as the case in the present work. In this work, thermal modeling is conducted with the use of a simple three-node thermal model, in which the temperature profile at hotspots is predicted. The equivalent circuit diagram of the corresponding thermal model is shown in Fig. 8. As shown in Fig. 9(a), the simulated winding temperature is in accordance with the measured value. The maximum temperature at the hotspots reaches 263°C, according to the simulated result.

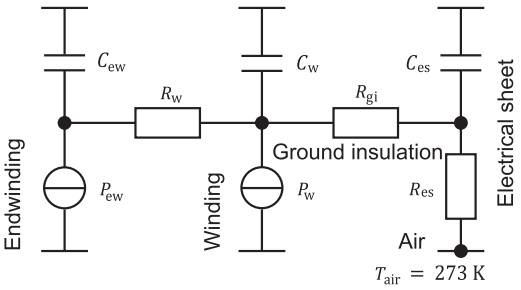

Fig. 8. Equivalent circuit diagram of the three-node thermal model

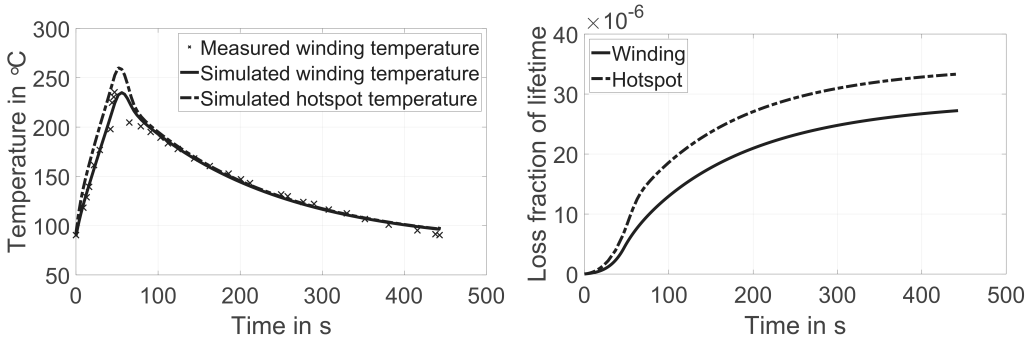

(a) (b)

Fig. 9. (a) Simulated temperature and (b) calculated loss fraction of lifetime at hotspots and windings

In the previous work [7], the Dakin-model is parameterized for the same motorette with three different temperatures. There, the lifetime at a constant temperature of 235°C is estimated to be 1059 h, with consideration of mechanical vibration and humidity effects. The related Dakin-constant B is characterized to be 3961.4 K. With values of the parameter B and the lifetime at a reference temperature of 235°C, the LF of the lifetime for the present work can be calculated according to (3). The calculated LFs of the lifetime at the winding and the hotspot are $0.027 \cdot 10^{-3}$ and $0.033 \cdot 10^{-3}$ for a single thermal cycle, respectively, as demonstrated in Fig. 9(b). This means, 37037 and 30303 thermal cycles are expected before a failure occurs for the winding and endwinding, respectively, without considering thermal-mechanical effects.

It seems that the rates of thermal degradation at the endwinding and winding do not show much difference in this case, this is probably because of the simplified slot configuration of the applied motorette. In practice, the slot configuration of an electric machine is more complex than the configuration of a motorette. A larger temperature gradient may occur across the winding. Therefore, it is meaningful to study the temperature distribution across the windings.

Besides, a comparison of experimental measurement and numerical calculation according to (3) is shown in Table 2. It is obvious that the calculated lifetime which considers only thermal aging is significantly longer than the experimental result. Therefore, a conclusion can be drawn that except for thermal aging, thermal-mechanical aging may also play an important role during a dynamic thermal loading process. Subsequently, the thermally induced mechanical stress is analyzed for a full understanding of associated aging mechanisms during a dynamic thermal process.

Table 2. Comparison of experimental and calculated lifetime

Method	Lifetime in cycle	Description
Experiment	$\overline{L} = 660, 423 < L_{95} > 807$	All aging factors considered
Calculation (hotspot)	30303	Only thermal aging considered
Calculation (winding)	37037	Only thermal aging considered, hotspots not considered

$\overline{L}$ – average lifetime; L_{95} – lifetime with 95% confidence

3.3. Analysis of thermal-mechanical stress with FEA method

To estimate the associated thermal-mechanical stress in the winding, a 3-dimensional finite element model of a single wire is built in *Ansys Workbench* for the study. Because of symmetry, only one-quarter of the round wire is applied for the simulation. As shown in Fig. 10, the geometry of the model is based on the Damid 200 GR2 material applied in the motorette for the winding. Analogous to the aforementioned 3-layer bonded model (Fig. 5), from inside out the three layers correspond to copper, PAI wire coating and Epoxy as impregnation material, respectively. Material data used for the simulation are listed in Table 3 [3].

The freedom of thermal expansion of the single wire model is correlated to the copper fill factor. A low filling factor provides more space for material expansion while a high filling factor results in limited expansion. In the present work, two extreme conditions are applied for the

Table 3. Material data used for the single wire model [3]

Parameter	Epoxy 4260	PAI	Copper
Young's modulus (MPa)	3500	7400	110E03
Poisson's ratio	0.44	0.42	0.34
Yield strength (MPa)	–	125	280
Ultimate tensile strength (MPa)	65	250	430
CTE (ppm/K)	70	16	18
Thermal conductivity (W/(m · K))	0.5	0.2	400

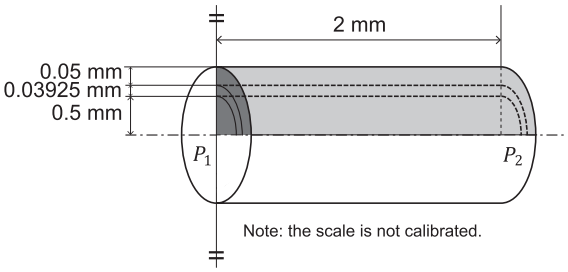

Fig. 10. Geometry of the single wire model

simulation, one with a very high filling factor and the other one with a very low filling factor, as schematically shown in Fig. 11. Assuming that one-quarter of a single wire in the middle area of the slot is selected, its expansion due to temperature change is limited by four boundaries, as numbered from 1 to 4 in Fig. 11. Since boundaries 1 and 2 lie on the axes of symmetry of the round wire, it is considered that the material lying on boundaries 1 and 2 may only expand along radial directions. For the case with a high copper fill factor, the wire can hardly expand in any direction, this means boundary 3 and 4 can be treated as locked. In comparison, a low copper fill factor means that the wire can expand freely in all directions. Thus, the wire is not restricted to boundary 3 and 4. During simulation under both boundary conditions, one end of the wire model is fixed as a symmetric plane (plane P_1 in Fig. 10), while the other end (plane P_2 in Fig. 10) is free to move. A heat source is added to the copper so that the wire temperature increases from

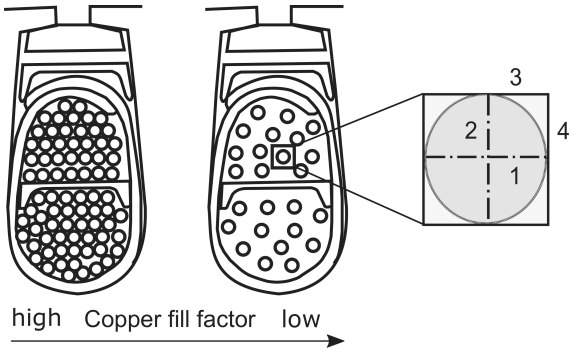

Fig. 11. Demonstration of the influence of copper fill-factor on the boundary conditions of single wire simulation (1, 2, 3, 4 denote boundaries for one-quarter of the wire)

90°C to 235°C within 47 s, which is consistent with the aforementioned experimental setting. The maximum stress value occurs at the free end of the wire model at a temperature of 235°C. The simulated von Mises stress between copper and PAI along the wire length reaches its maximum near the free end in both cases, as summarized in Table 4.

Table 4. Simulated mechanical stress in the PAI layer of the single wire model

Boundary condition	**Max. von Mises stress in PAI (MPa)**
Boundary 3 and 4 free	18
Boundary 3 and 4 fixed	183

Considering a yield strength of about 125 MPa and an ultimate stress of 250 MPa for the PAI material, it can be concluded that the wire coating is undergoing an elastic deformation when the copper fill factor is low. According to the S–N curve of PAI, as demonstrated in Fig. 6, the corresponding cycles resulting in cumulative fatigue are beyond 10^7, which means that the associated material fatigue is negligible in this case. In comparison, with a higher copper fill factor, a high thermal-mechanical stress of about 183 MPa can be generated, which means that the material undergoes a plastic deformation and will fail soon. Accordingly, about 300 cycles are required for a mechanical failure (Fig. 6). In comparison with the experimental result of 660 cycles in average, it therefore can be predicted that the dominant aging mechanism might shift from thermal to thermal-mechanical aging with an increasing copper fill factor.

The finite element single wire model introduced above provides a rough estimation of the thermal-mechanical stress under certain dynamic thermal process conditions. Besides, with the help of fatigue model, the significance of the associated thermal-mechanical aging is obtained. For a precise lifetime estimation regarding thermal-mechanical aging, additional effort is required with respect to material characterization. For example, the S–N curve should not only be obtained under tensile tests, other types of mechanical aging such as bending and compression should also be taken into consideration. Besides, the material data (Table 3) used for the finite element model are not in complete agreement with that of the applied insulating materials.

4. Conclusions

In the present work, experiments are conducted to simulate the dynamic loading process. The lifetime of the applied insulation system is estimated. To evaluate the thermal aging and thermal-mechanical aging separately, the associated thermal lifetime is calculated based on a modified Dakin model. Especially, for a precise evaluation of thermal aging, the temperature distribution at hotspots is simulated and used to evaluate thermal aging for the worst case. Through comparison of experimental and numerically calculated results, it can be concluded that not only thermal aging but also thermal-mechanical aging plays an important role during the dynamic thermal process. To estimate the associated thermal-mechanical stress, a 3D finite element single wire model is built. It indicates that the resulting thermal-mechanical stress is highly dependent on the copper fill factor. Especially for a machine with a high copper fill factor, the influence of thermal-mechanical stress on the winding aging should be considered.

In future work, the time-dependence of the resulting thermal-mechanical stress during the dynamic loading process will be studied. Besides, in terms of computational modeling, it will be focused on the extension of the single wire model, a model that allows one to consider the stress distribution inside the entire slot.

References

[1] Stone G.C., Boulter E.A., Culbert I., Dhirani H., *Electrical insulation for rotating machines: design, evaluation, aging, testing, and repair*, John Wiley & Sons (2004).

[2] Rothe R., Hameyer K., *Life expectancy calculation for electric vehicle traction motors regarding dynamic temperature and driving cycles*, 2011 IEEE International Electric Machines and Drives Conference (IEMDC), Niagara Falls, ON, Canada, pp. 1306–1309 (2011).

[3] Huang Z., *Modeling and testing of insulation degradation due to dynamic thermal loading of electrical machines*, Licentiate Thesis, Lund University, Lund (2017).

[4] Chen W., Nelson C., *Thermal stress in bonded joints*, IBM Journal of Research and Development, vol. 23, no. 2, pp. 179–188 (1979).

[5] Arrhenius S., *On the heat of dissociation and the influence of temperature on the degree of dissociation of the electrolytes*, Zeitschrift für Physikalische Chemie (in German, *Über die Dissociationswärme und den Einfluss der Temperatur auf den Dissociationsgrad der Elektrolyte*), vol. 4, no. 1, pp. 96–116 (1889).

[6] Dakin T.W., *Electrical insulation deterioration treated as a chemical rate phenomenon*, Transactions of the American Institute of Electrical Engineers, vol. 67, no. 1, pp. 113–122 (1948).

[7] Ruf A., Pauli F., Schröder M., Hameyer K., *Lifetime modelling of non-partial discharge resistant insulation systems of electrical machines in dynamic load collectives*, e & i Elektrotechnik und Informationstechnik (in German, *Lebensdauermodellierung von nicht-teilentladungsresistenten isoliersystemen elektrischer maschinen in dynamischen lastkollektiven*), vol. 135, no. 2, pp. 131–144 (2018).

[8] Pauli F., Schröder M., Hameyer K., *Design and evaluation methodology for insulation systems of low voltage drives with preformed coils*, 2019 9th International Electric Drives Production Conference (EDPC), Esslingen, Germany, pp. 1–7 (2019).

[9] Madonna V., Giangrande P., Lusuardi L., Cavallini A., Gerada C., Galea M., *Thermal overload and insulation aging of short duty cycle, aerospace motors*, IEEE Transactions on Industrial Electronics, vol. 67, no. 4, pp. 2618–2629 (2019).

[10] Sciascera C., Galea M., Giangrande P., Gerada C., *Lifetime consumption and degradation analysis of the winding insulation of electrical machines*, 2016 8th IET International Conference on Power Electronics, Machines and Drives (PEMD), Glasgow, UK, pp. 1–5 (2016).

[11] IEC 60505, *Evaluation and qualification of electrical insulation systems* (2011).

[12] Ruf A., Paustenbach J., Franck D., Hameyer K., *A methodology to identify electrical ageing of winding insulation systems*, 2017 IEEE International Electric Machines and Drives Conference (IEMDC), Miami, FL, USA, pp. 1–7 (2017).

[13] Pauli F., Ruf A., Hameyer K., *Low voltage winding insulation systems under the influence of high du/dt slew rate inverter voltage*, Archives of Electrical Engineering, vol. 69, no. 1, pp. 187–202 (2020).

[14] IEC 60034–18–41, *Rotating electrical machines – Part 18–41: Partial discharge free electrical insulation system (Type I) used in rotating electrical machines fed from voltage converters – Qualification and quality control tests* (2014).

[15] Nikolova G., Ivanova J., *Interfacial shear and peeling stresses in a two-plate structure subjected to monotonically increasing thermal loading*, Journal of Theoretical and Applied Mechanics, vol. 51 (2013).